Published in the Proceedings of the 16th International Aluminum Alloys Conference (ICAA16) 2018
ISBN: 978-1-926872-41-4
by the Canadian Institute of Mining, Metallurgy & Petroleum

EFFECTS OF SECOND-PHASE PARTICLE SIZE ON THE HIGH-TEMPERATURE DUCTILITY OF Al-Mg SOLID SOLUTION ALLOYS CONTAINING SMALL AMOUNTS OF IMPURITY ATOMS

*T. Ito[1], H. Fujiwara[1], K. Kawasaki[1], and T. Mizuguchi[2]

[1]National Institute of Technology, Kagawa College
Takamatsu, Kagawa, Japan
(Corresponding author: t-ito@t.kagawa-nct.ac.jp)

[2]Ehime University
Matsuyama, Ehime, Japan

ABSTRACT

In this study, we characterize the high-temperature deformation of typical "Class I" solid solution Al-Mg alloys as a superplastic elongation attributable to the solute drag creep of dislocations. The second-phase particles formed by adding Fe or Si as impurity atoms to the Al-Mg alloys impeded the gliding motion of dislocations, thereby decreasing their hot ductility and resulting in cavity formation. High-temperature tensile tests were performed with initial strain rates in the range of 1×10^{-3} to 1×10^{-1} s^{-1} at air temperatures 673–723 K. The dominant high-temperature deformation mechanism in these alloys was the solute drag creep controlled by the interdiffusion of Mg in Al. In this study, the calculation of critical length, defined by the diffusion-based relaxation of the stress concentration region around second-phase particles, is reported using the Needleman–Rice parameter. An analysis of the impact of cavity formation based on a comparison of the Needleman–Rice parameter and second-phase particle size is also reported.

KEYWORDS

Al-Mg alloy, High-temperature ductility, Impurity atom, Particle size, Second-phase, Solute drag creep

INTRODUCTION

Aluminum alloys with high specific strengths are utilized as structural materials for transportation machines to minimize their weight, which consequently maximizes fuel efficiency, environment preservation, and so on (Miller et al., 2000; Heinz et al., 2000; Starke & Staley, 1996; Polmear, 1996; Immarigeon et al., 1995; Burger, Gupta, Jeffrey, & Lloyd, 1995; Ye, 2003). Microstructure refinement by severe plastic deformation (SPD) has been performed on a laboratory scale to achieve a higher strength of crystalline materials (Valiev et al., 2006; Song, Ponge, Raabe, Speer, & Matlock, 2006; Beyerlein & Toth, 2009; Sabirov, Murashkin, & Valiev, 2013; Sauvage, Wilde, Divinski, Horita, & Valiev, 2012). At room temperature, grain refinement strengthens the material, as given by the Hall-Petch relationship (Hall, 1951; Petch, 1953); at higher temperatures, superplasticity can be expected（Sherby & Wadsworth, 1989; Edington, Melton, & Cutler, 1979; Furukawa, Horita, Nemoto, & Langdon, 2001; Langdon, 2006). However, the synthesis of large-size materials by SPD processes is not yet feasible.

Superplastic forming of aluminum alloys has been considered (Boyer, 1996; Barnes, 2007); however, in addition to the high costs of such materials, this is discouraged by the cold formability of aluminum when compared to steel (Boyer, 1996; Barnes, 2007). This could cause grain boundary sliding (GBS) in aluminum alloys (Langdon, 2006). However, Taleff et al. (1996; 1998; 1999) and authors et al. (Ito, Shibasaki, Koma, & Otsuka, 2002; Ito, Koma, Shibasaki, & Otsuka, 2002) have reported on a superplastic-like behavior controlled by intragranular deformation. The dominant deformation mechanism of this superplastic-like behavior is solute drag creep, which is typical of Class I solution alloys (Cannon, & Sherby, 1970; Weertman, 1957; Weertman, 1977) or Class A solution alloys (Mohamed, & Langdon, 1974; Vagarali, & Langdon, 1981; Yavari, & Langdon, 1982; Yavari, Mohamed, & Langdon, 1981; Endo, Shimada, & Langdon, 1984). Ito et al. (2002) have reported a large elongation of over 400% by transgranular deformation without recrystallization in an Al-Mg solid solution single crystal alloy. This result can be expected in the hot working of aluminum alloys because of their high elongations irrespective of the grain refinement processes. The Al-Mg alloys formed through a hot-blow process in the solute drag creep region were utilized as one of the structural parts in Honda Legend (Furukawa-Sky, 2008).

Furthermore, second-phase particles may decrease ductility because they disturb the movement of dislocations in solute drag creep, facilitating stress concentration and cavity formation. The presence of impurity atoms may decrease ductility by solute drag creep, because the recycle rate tends to increase, especially in aluminum alloys. Previous studies (Ito, Kawasaki, & Mizuguchi, 2016) have investigated the hot ductility of Al-Mg solid solution alloys with impurity atoms of Cr and Mn. This paper reports the hot ductility of Al-Mg solid solution alloys with Fe or Si impurities.

METHODS

Materials

Hot-rolled sheets of Al-3wt%Mg alloys of 1 mm thickness were used in this study. The chemical compositions of the alloys are shown in Table 1. To investigate the effects of second-phase particles, model alloys of Fe, Si, and Fe + Si were prepared. For comparison, Al-Mg basic alloy with few impurity atoms was prepared. An ingot of 30 mm thickness and 80 mm width was subjected to homogenization treatment at a temperature of 773 K for 43.2 ks. The thickness of the top and bottom surfaces were hot rolled to a thickness of 4 mm (reduction rate: 60%), and was then cold rolled to a thickness of 1 mm (reduction rate: 90%), and finally final annealing was conducted at 723 K for 60 s in a salt bath.

Table 1. Chemical compositions of studied alloys

Alloys	Elements	Mg	Fe	Si	Mn	Cr	Ti	Zn	Cu	Al
Al-Mg	wt %	2.96	0.08	0.04	0.00	0.00	0.02	0.01	0.00	bal.
	at %	3.28	0.04	0.04	0.00	0.00	0.01	0.00	0.00	bal.
Al-Mg-Fe	wt %	2.90	0.32	0.03	0.00	0.01	0.02	0.00	0.00	bal.
	at %	3.21	0.15	0.03	0.00	0.01	0.01	0.00	0.00	bal.
Al-Mg-Si	wt %	2.96	0.08	0.20	0.00	0.00	0.02	0.00	0.00	bal.
	at %	3.28	0.04	0.19	0.00	0.00	0.01	0.00	0.00	bal.
Al-Mg-Fe-Si	wt %	3.01	0.33	0.20	0.00	0.01	0.01	0.00	0.00	bal.
	at %	3.34	0.16	0.19	0.00	0.01	0.01	0.00	0.00	bal.

High-Temperature Tensile Tests

To investigate the hot ductility of this alloy, high-temperature tensile tests were conducted. The tensile test specimens were machined with their stress axes parallel to the rolling direction (RD). The dimensions of the tensile test specimens are shown in Figure 1. High-temperature tensile test machine of Illinois Tool Works Inc. (Model: Instron 5586) was used. The high-temperature tensile tests were conducted in the air at an initial strain rate range of 1×10^{-2} to 1×10^{-1} s^{-1} and at temperature range of 673 to 723 K. The specimens were loaded in an electric furnace, whose temperature was gradually increased until the specified test temperature was reached. This temperature was maintained for 15 min to stabilize the specimen before the test was started.

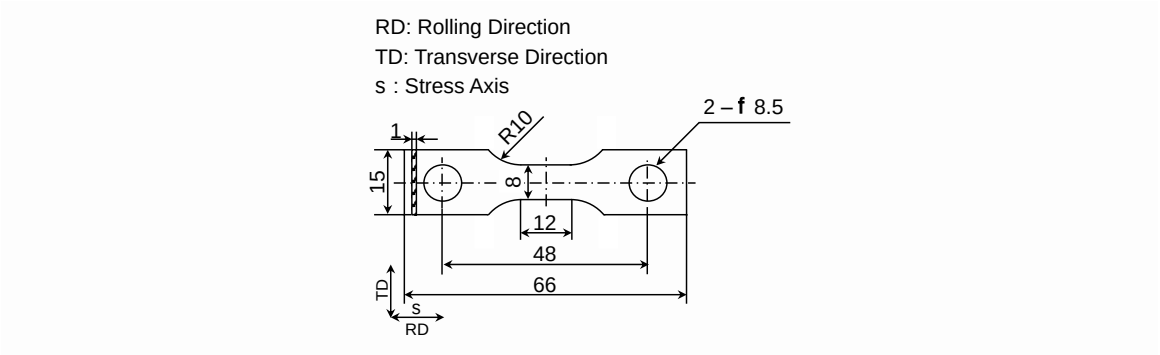

Figure 1. Dimensions of high-temperature tensile test specimen

Microstructure Observations

To investigate the microstructural characteristics of these alloys, the microstructure was examined using field-emission type scanning electron microscopy (FE-SEM: Hitachi High-Technologies; Model: SU-70), electron back scatter diffraction (EBSD: AMETEK Inc.), and energy dispersive X-ray spectrometry (EDX: AMETEK Inc.) for this study. The average grain sizes in these alloys were determined by EBSD method. In addition, the second-phase particles, formed by the addition of impurity atoms, were observed using FE-SEM and EDX. The surface of the microstructure was adequately polished using water-proof emery paper (#800 to #4000), buff polished with a diamond paste of 3 μm grain size, and electropolished in a solution of ethanol, perchloric acid, and ethylene glycol, 7:2:1,. Electropolishing was performed for 30 s at a temperature of about 267 K, direct voltage 20 V, and direct current about 1 A. the EBSD measurements were conducted at an acceleration voltage of 20 kV, area 750 μm × 750 μm, and beam distance 1.4 μm. The EDX, surface and point analyses were carried out at an acceleration voltage of 20 kV.

RESULTS AND DISCUSSION

Initial Microstructures

The microstructures of each alloy for as received samples and just before of the high-temperature tensile tests are shown in Figure 2. During the high-temperature tensile tests, the alloys were held for 15 min at test temperatures and then quenched. The average grain sizes as received samples and just before of the high-temperature tensile tests are shown in Table 2. Table 2 shows that the average grain sizes of each alloy for the tested specimens are about 20 to 30 μm, but the sizes before the high-temperature tensile tests are different as a result of the altered thermal stability of the microstructures. The microstructures of Al-Mg and Al-Mg-Si alloys are thermally unstable and grain growth occur at high-temperature region. The microstructures of Al-Mg-Fe and Al-Mg-Fe-Si alloys are thermally stable and fine-grained equiaxed microstructures below 40 μm are maintained at test temperature regions. However, the microstructures of each alloy at a temperature of 673 K are thermally stable, with average grain sizes of about 20 to 30 μm.

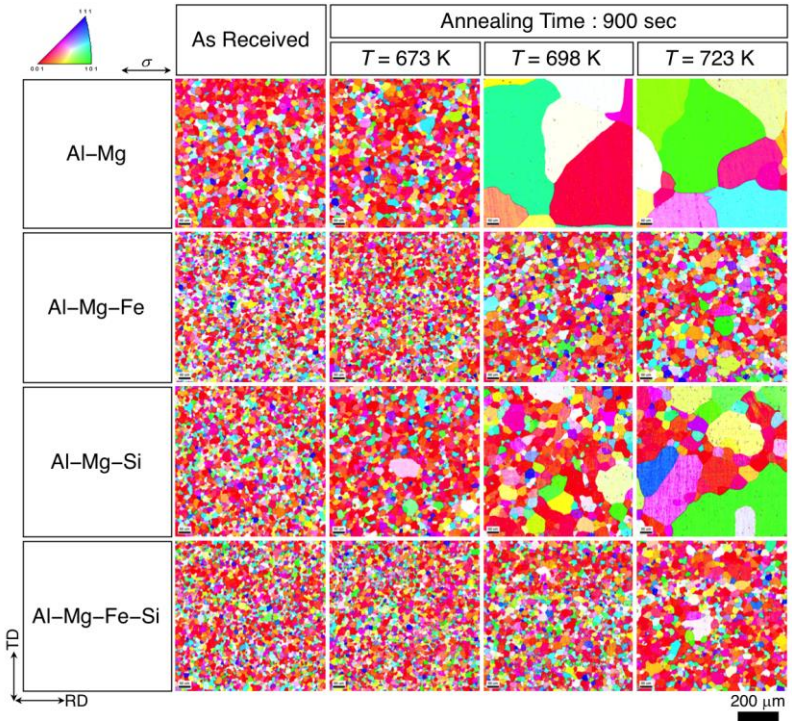

Figure 2. Microstructures of Al-Mg alloys as received samples and just before of high-temperature tensile test

Table 2. Average grain sizes of Al-Mg alloys as received samples and just before of high-temperature tensile tests

Alloys	Average Grain Sizes, d / μm			
	As Received	Just Before High Temperature Tensile Tests		
		T = 673 K	T = 698 K	T = 723 K
Al–Mg	32.9 ± 1.9	31.3 ± 3.1	364 ± 113	312 ± 31
Al–Mg–Fe	19.1 ± 1.1	19.5 ± 3.0	30.2 ± 2.7	34.9 ± 2.6
Al–Mg–Si	21.5 ± 0.6	31.3 ± 0.8	59.2 ± 7.7	218 ± 252
Al–Mg–Fe–Si	17.9 ± 0.4	20.0 ± 3.7	23.9 ± 0.2	37.2 ± 3.2

On the other hand, the area fractions and average sizes of the second-phase particles that exist in each alloy are shown in Table 3. The area fraction of second-phase particles for the Al-Mg alloy is about 1.3%, but for the impurity atoms it varies from 2 to 3%. The area fraction of the second-phase particles in Al-Mg-Fe alloys is low as a result of the polishing. Therefore, the fractions of second phase particles in the alloys with impurity atoms are larger than that of Al-Mg basic alloy, and this could affect ductility at high temperature. However, the average sizes of second-phase particles are about 1 μm at each alloy.

Table 3. Area fractions and average particles sizes of second-phase particles in Al-Mg alloys

Alloys	Area Fractions of Second-Phase Particles, ϕ (%)	Average Particle Sizes of Second-Phase Particles, d_p / μm
Al–Mg	1.29 ± 0.01	0.82 ± 0.20
Al–Mg–Fe	0.56 ± 0.00	0.95 ± 0.20
Al–Mg–Si	2.49 ± 0.02	1.20 ± 0.43
Al–Mg–Fe–Si	2.81 ± 0.01	1.08 ± 0.51

Hot Ductility

Figure 3 shows the elongation to fracture as a function of the initial strain rate for each alloy. A high ductility of over 200% is obtained at the test conditions. However, the elongation to fracture at temperatures of 698 K and 723 K for Al-Mg and Al-Mg-Si alloys, respectively, is below 200%. Figure 3 shows fine and coarse-grained microstructure of the alloys under the test conditions; thus, it can be said that a non-uniform deformation in the blended microstructures decreased their ductility.

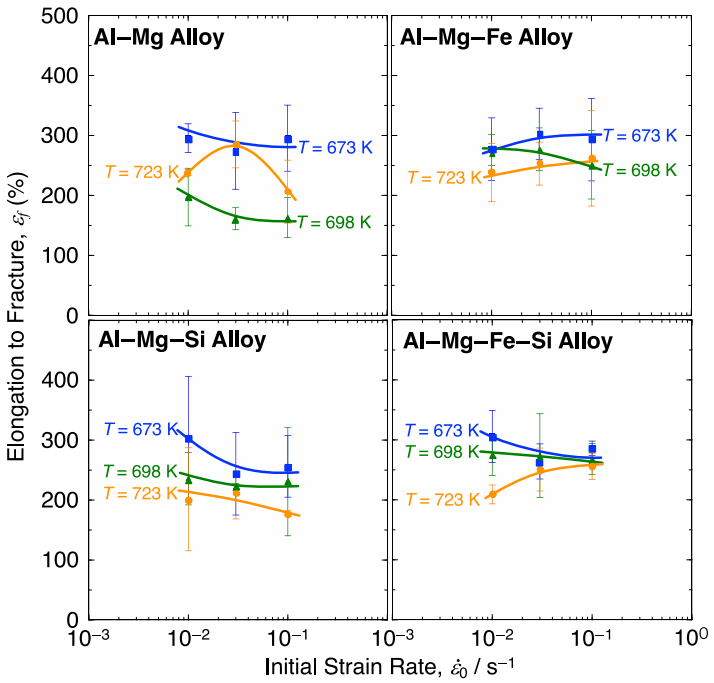

Figure 3. Elongation to fracture as a function of initial strain rate for Al-Mg alloys

High-Temperature Deformation Mechanism

To describe high-temperature deformation mechanism, the following constitutive equation is generally used (Bird, Mukherjee, & Done, 1969):

$$\dot{\varepsilon} = A\sigma^{n}\exp\left(-\frac{Q}{RT}\right), \tag{1}$$

where, $\dot{\varepsilon}$ is the strain rate, A is the materials constant, σ is the stress, Q is the activation energy for deformation, R is the gas constant, and T is the absolute temperature.

From equation (1), Figure 4 shows double logarithmic plot of initial strain rate vs. tensile stress for each alloy. The slope of straight lines corresponds to the stress exponent. The stress exponent of each alloy shows about 3.5 despite the presence of second-phase particles. This value agrees with the stress exponent for solute drag creep (Weertman, 1957).

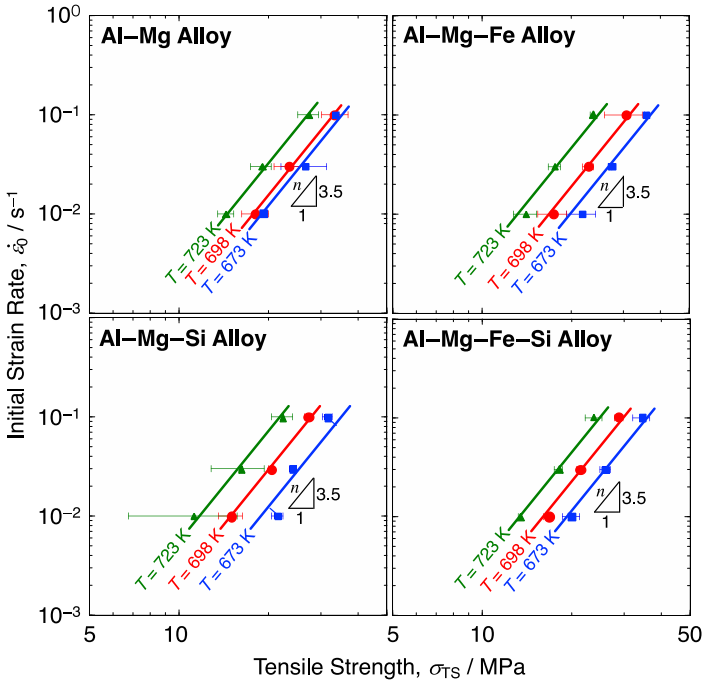

Figure 4. Initial strain rate as a function of tensile strength for Al-Mg alloys

To discuss on the high-temperature deformation mechanism of each alloy, activation energy for deformation was calculated, and it is shown as equation (2).

$$Q = nR\frac{\partial \ln s}{\partial (1/T)} \tag{2}$$

To calculate the activation energy for deformation, the stresses that cross-cut at the initial strain rate of 3×10^{-2} s^{-1} in Figure 5 are used for each alloy. Here, Arrhenius plots are used to determine the activation energy for deformation. The activation energy for deformation can be calculated by multiplying the stress exponent (n = 3.5), gas constant, and slope of the plot. The activation energies for deformation of Al-Mg, Al-Mg-Fe, Al-Mg-Si, and Al-Mg-Fe-Si alloys were 109, 134, 125, and 115 kJ/mol, respectively. These values are close to the activation energy for interdiffusion of Mg in Al (122 kJ/mol) (Minamino et al., 1983). Therefore, solute drag creep can be considered a dominant deformation mechanism in these alloys, controlled by interdiffusion of Mg in Al. In other words, it has been proven that the dominant deformation mechanism was solute drag creep irrespective of the additional alloys present in the second-phase particles. This result is on the basis of the comparatively low area fraction of the second-phase particles.

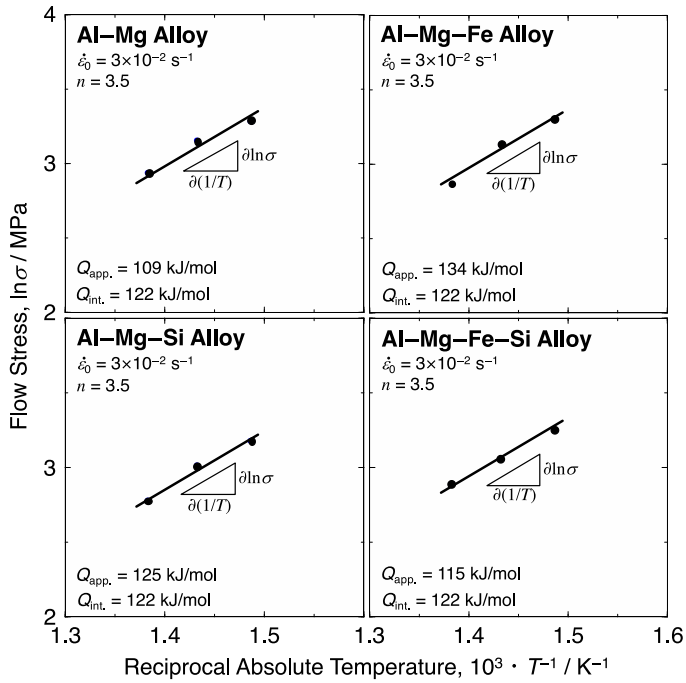

Figure 5. Arrhenius plots of flow stress vs. reciprocal absolute temperature for Al-Mg alloys

Effects of Second-Phase Particles for Hot Ductility

Needlemen and Rice (1980) suggested a critical length (Λ) over which stress concentrations around second-phase particles are rapidly reduced by diffusional relaxation during high-temperature deformation. According to them, the critical length for the second-phase particles present the intergranular (Λ_{gb}) or transgranular deformation (Λ_L) can be expressed by following equations.

$$\Lambda_{gb} = \left\{ \frac{\Omega D_{gb} \delta \sigma}{kT\dot{\varepsilon}} \right\}^{1/3} \tag{3}$$

$$\Lambda_L = \left\{ \frac{\Omega D_L \sigma}{\pi kT\dot{\varepsilon}} \right\}^{1/2} \tag{4}$$

Where, Λ is the critical length (Needleman-Rice parameter), Ω is the atomic volume, k is the Boltzmann constant, T is the absolute temperature, δ is the width of grain boundary, π is the circumstance, D_{gb} is the grain boundary diffusion coefficient, D_L is the lattice diffusion coefficient, σ is the stress, and $\dot{\varepsilon}$ is the strain rate.

Therefore, the difficulty in cavity formation could be attributed to the stress concentration generated around the second-phase particles; this can be addressed by atomic diffusion if the size of the second-phase particles are smaller than two times of critical length (2Λ). Figure 6 shows the Needleman-Rice parameter (2Λ) as a function of $\sigma/\dot{\varepsilon}$ for Al-Mg alloys with a thermally stable microstructure at a temperature of 673 K, according to the equations (3) and (4). To construct Figure 6, the following values (Frost, & Ashby, 1982) were used: $\Omega = 2.49\times10^{-10}$ m^3, $\delta D_{gb} = 1.51\times10^{-20}$ m^3/s, and $D_L = 1.62\times10^{-15}$ m^2/s. The rough indications of strain rates are represented by broken lines in Figure 6. From Figure 6, the critical length (2Λ) over which the stress concentration can be relaxed are 0.4 to 0.8 μm, and 0.03 to 0.1 μm for grain boundary and transgranular deformation, respectively. The average sizes of the second-phase particles of each alloy in this study were about 1 μm. The extent of stress reduction around

second-phase particles was difficult to estimate, taking into account the critical length. Cavity formation was not totally avoided. However, a superplastic-like behavior (over 200% elongation) was observed. Therefore, it would be thought that the superplastic-like elongation by solute drag creep over 200% is obtained, because the area fraction of second-phase particles are a little less than 3%.

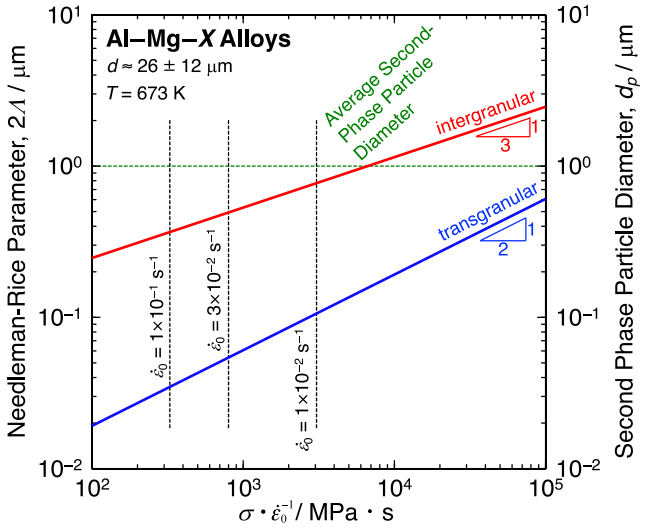

Figure 6. Needleman-Rice parameter as a function of s · $\dot{\varepsilon}_0^{-1}$ for Al-Mg alloys

CONCLUSIONS

Effects of second-phase particle sizes on hot ductility of Al-Mg irrespective of the addition of impurity atoms were investigated, and the following results were obtained.

[1] The average grain sizes of each alloy just before high-temperature tensile tests were about 20 to 30 μm. However, the microstructures of Al-Mg, and Al-Mg-Si alloys were thermally unstable, the microstructures were occurred the grain growth before high-temperature tensile tests. Moreover, the microstructures of each alloy consisting of these grain sizes are difficult to the occurrence the grain boundary sliding that is dominant deformation mechanism of superplastic phenomena.

[2] The average grain sizes of the second-phase particles existing in each alloy are about 1 μm, and their area fraction is less than 3%.

[3] Large elongations of over 200% were obtained in the wide test conditions of each alloy.

[4] From the viewpoint of stress exponent and activation energy for deformation, the dominant deformation mechanism that is obtained the large elongation would be thought the solute drag creep that is rate-controlled by the interdiffusion of Mg in Al.

[5] The second-phase particle sizes existing in these alloys would be easily occurred the cavity defect formation from viewpoint of the Needleman-Rice parameter, but it would be thought that the superplastic-like elongation over 200% is obtained, because the area fraction of second-phase particles are a little less than 3%.

ACKNOWLEDGMENTS

This work was supported by JSPS KAKENHI, Grant Number JP15K06494. Authors show great appreciation to this support.

REFERENCES

Barnes, A. J. (1994). Superplastic Forming of Aluminum Alloys. *Materials Science Forum*, *170–172*, 701–714. https://doi.org/10.4028/www.scientific.net/MSF.170-172.701

Barnes, A. J. (2007). Superplastic forming 40 years and still growing. *Journal of Materials Engineering and Performance*, *16* (4), 440–454. https://doi.org/10.1007/s11665-007-9076-5

Beyerlein, I. J, & Toth, L. S. (2009). Texture evolution in equal-channel angular extrusion. *Progress in Materials Science*, *54* (4), 427–510. https://doi.org/10.1016/j.pmatsci.2009.01.001

Bird, J. E., Mukherjee, A. K., & Done, J. E. (1969). Correlations between high-temperature creep behavior and structure. In Brandon, D. G., & Rosen, A. (Eds), *Quantitative relation between property and microstructure* (pp. 255–342). Israel Universities Press.

Boyer, R. R. (1996). An overview on the use of titanium in the aerospace industry. *Materials Science & Engineering*, *A213* (1-2), 103–114. https://doi.org/10.1016/0921-5093(96)10233-1

Burger, G. B., Gupta, A. K., Jeffrey, P. W., & Lloyd, D. J. (1995). Microstructural control of aluminum sheet used in automotive applications. *Materials Characterization*, *35* (1), 23–39. https://doi.org/10.1016/1044-5803(95)00065-8

Cannon, W. R., & Sherby, O. D. (1970). High-temperature creep behavior of class I and class II solid solution alloys. *Metallurgical Transaction*, *1* (4), 1030–1032. https://doi.org/10.1007/BF02811789

Edington, J. W., Melton, K. N., & Cutler, C.P. (1979). Superplasticity. *Progress in Materials Science*, *21* (1,2), 61–170. https://doi.org/10.1016/0079-6425(76)90005-0

Endo, T., Shimada, T., & Langdon, T. G. (1984). The deviation from creep by viscous glide in solid solution alloys at high stresses-I. Characteristics of the dragging stress. *Acta Metallurigica*, *32* (11), 1991–1999. https://doi.org/10.1016/0001-6160(84)90179-2

Frost, H. J., & Ashby, M. F. (1982). *Deformation-mechanism maps*. Oxford: Pergamon Press.

Furukawa, M., Horita, Z., Nemoto, M., & Langdon, T.G. (2001). Processing of metals by equal-channel angular pressing. *Journal of Materials Science*, *36* (12), 2835–2843. https://doi.org/10.1023/A:1017932417043

Furukawa-Sky. (2008). High-temperature forming technology for aluminum alloys. *Frukawa-Sky Review*, *(4)*, 66–69.

Hall, E. O. (1951). The Deformation and Aging of Mild Steel: III Discussion of Results. *Proceedings of the Physical Society. Section B*, *64* (9), 747–753. https://doi.org/10.1088/0370-1301/64/9/303

Heinz, A., Haszler, A., Keidel, C., Moldenhauer, S., Benedictus, R., & Miller,W. S. (2000). Recent development in aluminum alloys for aerospace applications. *Materials Science & Engineering*, *A280* (1), 102–107. https://doi.org.10.1016/S0921-5093(99)00674-7

Immarigeon, J-P., Holt, R. T., Koul, A. K., Zhao, L., Wallace, W., & Beddoes, J. C. (1995). Lightweight materials for aircraft applications. *Materials Characterization*, *35* (1), 41–67. https://doi.org/10.1016/1044-5803(95)00066-6

Ito, T., Shibasaki, S., Koma, M., & Otsuka, M. (2002). Superplastic-like behavior in medium grained and single crystalline Al-Mg solid solution alloys. *Journal of the Japan Institute of Metals*, *66* (4), 409–417. https://doi.org/10.2320/jinstmet1952.66.4_409

Ito, T., Koma, M., Shibasaki, S., & Otsuka, M. (2002). Superplastic-like behavior for Al-Mg alloys with high concentration of magnesium. *Journal of the Japan Institute of Metals*, *66* (5), 476–484. https://doi.org/10.2320/jinstmet1952.66.5_476

Ito, T., Kawasaki, K., & Mizuguchi, T. (2016). Influence of second-phase particles on the hot ductility of Al-Mg solid solution alloys. *Materials Science Forum*, *838-839*, 249–255. http://doi.org/10.4028/www.scientific.net/MSF.838-839.249

Langdon, T. G. (2006). Grain boundary sliding revisited: Developments in sliding over four decades. *Journal of Materials Science*, *41* (3), 597–609. https://doi.org/10.1007/s10853-006-6476-0

Miller, W. S., Zhuang, L., Bottema, J., Wittebrood, A. J., De Smet, P., Haszler, A., & Vieregge, A. (2000). Recent development in aluminum alloys for the automotive industry. *Materials Science & Engineering*, *A280* (1), 37–49. https://doi.org/10.1016/S0921-5093(99)00653-X

Minamino, Y., Yamane, T., Shimomura, A., Shimada, M., Koizumi, M., Ogawa, N., Takahashi, J., & Kimura, H. (1983). Effect of high pressure on interdiffusion in am Al-Mg alloy. *Journal of Materials Science*, *18* (9), 2679–2687. https://doi.org/10.1007/BF00547584

Mohamed, F. A., & Langdon, T. G. (1974). The transition from dislocation climb to viscous glide in creep of solid solution alloys. *Acta Metallurgica*, *22* (6), 779–788. https://doi.org/10.1016/0001-6160(74)90088-1

Needleman, A., & Rice, J. R. (1980). Plastic creep flow effects in the diffusive cavitation of grain boundaries. *Acta Metallurgica*, *28* (10), 1315–1332. https://doi.org/10.1016/0001-6160(80)90001-2

Petch, N. J. (1953). The Cleavage Strength of Polycrystals. *Journal of the Iron & Steel Institute*, *174* (5), 25–28.

Polmear, I. J. (1996). Recent developments in light alloys. *Materials Transactions, JIM*, *37* (1), 12–31. https://doi.org/10.2320/matertrans1989.37.12

Sabirov, I., Murashkin, M. Y., & Valiev, R. Z. (2013). Nanostructured aluminum alloys produced by severe plastic deformation: New horizons in development. *Materials Science & Engineering*, *A560*, 1–24. https://doi.org/10.1016/j.msea.2012.09.020

Sauvage, X., Wilde, G., Divinski, S. V., Horita, Z. & Valiev, R. Z. (2012). Grain boundaries in ultrafine grained materials processed by severe plastic deformation & related phenomena. *Materials Science & Engineering*, *A540*, 1–12. https://doi.org/10.1016/j.msea.2012.01.080

Sherby, O. D., & Wadsworth, J. (1989). Superplasticity-Recent advances and future directions. *Progress in Materials Science*, *33* (3), 169–221. https://doi.org/10.1016/0079-6425(89)90004-2

Song, R., Ponge, D., Raabe, D., Speer, J. G., & Matlock, D. K. (2006). Overview of processing, microstructure & mechanical properties of ultrafine grained bcc steels. *Materials Science & Engineering*, *A441* (1–2), 1–17. https://doi.org/10.1016/j.msea.2006.08.095

Starke, E. A., Jr., & Staley, J. T. (1996). Application of modern aluminum alloys to aircraft. *Progress in Aerospace Science*, *32* (2–3), 131–172. https://doi.org/10.1016/0376-0421(95)00004-6

Taleff, E. M., Lesuer, D. R., & Wadsworth, J. (1996). Enhanced ductility in coarse-grained Al-Mg alloys. *Metallurgical and Materials Transactions*, *A27* (2), 343–352. https://doi.org/10.1007/BF02648411

Taleff, E. M., Henshall, G. A., Nieh, T. G., Lesuer, D. R., & Wadsworth, J. (1998). Warm-temperature tensile ductility in Al-Mg alloys. *Metallurgical and Materials Transactions A*, *29* (13), 1081–1091. http://doi.org/10.1007/s11661-998-1017-x

Taleff, E. M., & Nevland, P. J. (1999). The high-temperature deformation and tensile ductility of Al alloys. *JOM*, *51* (5), 34–36. https://doi.org/10.1007/s11837-999-0009-7

Vagarali, S. S., & Langdon, T. G. (1981). Deformation Mechanism in h.c.p. metals at elevated temperatures-II. Creep behavior of a Mg-0.8%Al solid solution alloy. *Acta Metallurgica*, *30* (6), 1157–1170. https://doi.org/10.1016/0001-6160(82)90009-8

Valiev, R. Z., Estrin, Y., Horita, Z., Langdon, T. G., Zehetbauer, M. J., & Zhu, Y. T. (2006). Producing bulk ultrafine-grained materials by severe plastic deformation. *JOM*, *58* (4), 33–39. https://doi.org/10.1007/s11837-006-0213-7

Weertman, J. (1957). Steady-state creep of crystals. *Journal of Applied Physics*, *28* (10), 1185–1189. https://doi.org/10.1063/1.1722604

Weertman, J. (1977). Theory of internal stress for class I high-temperature creep alloys. *Acta Metallurgica*, *25* (12), 1393–1401. https://doi.org/10.1016/0001-6160(77)90070-0

Yavari, P., Mohamed, F. A., & Langdon, T. G. (1981). Creep and substructure formation in an Al-5%Mg solid solution alloy. *Acta Metallurgica*, *29* (8), 1495–1507. https://doi.org/10.1016/0001-6160(81)90184-X

Yavari, P., & Langdon, T. G. (1982). An examination of the breakdown in creep by viscous glide in solid solution alloys at high stress levels. *Acta Metallurgica*, *30* (12), 2182–2196. https://doi.org/10.1016/0001-6160(82)90139-0

Ye, H. (2003). An overview of the development of Al-Si−alloy based material for engine applications. *Journal of Materials Engineering and Performance*, *12* (3), 288–297. https://doi.org/10.1361/105994903770343132